POLITECNICO
MILANO 1863

SCUOLA DI INGEGNERIA INDUSTRIALE
E DELL'INFORMAZIONE

Magnetoelectric nanoparticles as innovative technology for motor nerve stimulation: feasibility assessment through computational methods

Tesi di Laurea Magistrale in
Biomedical Engineering - Ingegneria Biomedica

Valentina Galletta, 10602963

Advisor:
Prof. Paolo Ravazzani

Co-advisors:
Emma Chiaramello
Serena Fiocchi

Academic year:
2021-2022

Abstract: This study focuses on the assessment of the feasibility of using magnetoelectric nanoparticles (MENPs) for the stimulation of arm's peripheral nerves, aiming at demonstrating their potentiality as tools for the next generation of bionic interfaces for human arms. The analysis was performed by means of computational techniques, paring electromagnetic simulation, and neuronal dynamic simulation. Both simplified geometries and more realistic models were used in the simulations. Particularly, the level of detail, and so the complexity of the model, increased in the simulations. At first, a very simple framework, with a single nanoparticle and a single axon, was useful to explore the influence of the MENP on the neuron, the impact of the interposed tissue, and variations over the stimulus itself. Then, the appropriateness of using MENPs in more realistic frameworks was demonstrated. Results suggested the feasibility of the proposed technique, highlighting the high spatial resolution achievable by such nanostructures.

Key-words: Magnetoelectric nanoparticles, electrical nerve stimulation, numerical techniques.

1. Introduction

Electrical stimulation is the application of safe levels of electric current for medical purposes. The motor nerve stimulation elicits muscle contraction using electric pulses over the peripheral sensory-motor system, contributing to recovery functions, strengthening atrophied muscles, and relieving pain. [1–3].

In the recent past, peripheral neural interfaces, also known as neuroprostheses, have been successfully used for the neuromodulation of the autonomic nervous system and to restore sensory-motor functions in disabled subjects [4]. Neuroprostheses are devices that use electrical stimulation to activate the neuromuscular system to improve or substitute motor or sensory functions of an impaired CNS. [5]. It is possible to classify differently the neuroprostheses, depending on the usage time and the electrodes at the interface. Neuroprosheses can be used temporally, for rehabilitation, or permanently, for daily activities and lifetime tasks [5], whereas the already existing technologies to use at the interface are transcutaneous, percutaneous, or implanted (cuff or epimysial ones) electrodes [2, 3]. Due to their peculiarities, surface and percutaneous stimulation neuroprostheses could be better in rehabilitation use or for specific daily tasks whereas implantable neuroprostheses are preferable for chronic use.

Surface electrodes are placed on the skin over the targeted motor points of muscles in the vicinity of motor nerves that need to be stimulated. They are noninvasive, inexpensive, and simple to apply, however, they can lack selectivity for small and deep muscles, may cause skin irritation and pain (related to the electrode's size), and are often non-aesthetic [6, 7]. Percutaneous electrodes are instead placed close to the motor point of muscles, passing through the skin into target muscles. They can provoke a repeatable response over time with nonsurgical intervention and compared to transcutaneous electrodes, they have higher muscle selectivity. The risk of infection is low, but they can cause some granulomas [6, 7]. At last, implantable electrodes are placed around (cuff) muscle nerves or over (epimysial) muscles. They both overcome the main drawbacks of the previous electrodes regarding muscle selectivity and infections but they can address different problems related to their functioning [6, 7]. In fact, it is possible to distinguish three categories of failure mechanisms:

- Physiological criteria, such as poor recruitment properties, stimulus thresholds that are excessively high or low, poor repeatability, insufficient strength, and adverse sensations.
- Biological failures which are either mechanically induced at the surgical installation (excess encapsulation, infection or rejection) or induced with stimulation.
- Physical failures in relation to the conductor, such as electrochemical degradation or mechanical failures (breakage), and the insulator.

Over the last few years, the growing interest in electrical stimulation techniques with desirable high spatial and temporal resolution has led to a fast technological expansion, and a wide range of innovative technologies and materials has been developed. For example, light stimulation of neural tissue with thin film photoactive interfaces [8], memristor-based neuromodulation devices [9], ferromagnetic superparamagnetic iron oxide nanoparticles [10], and polymeric nanoparticles [11]. Recently, a class of materials that is gaining particular interest is multiferroic structures exhibiting the magnetoelectric (ME) effect, i.e., a linear coupling between the applied magnetic field and generated electric voltage [12]. Among different devices, magnetoelectric nanoparticles (MENPs) are gaining particular interest. Their high selectivity and fewer invasiveness will possibly overcome the actual drawbacks of the existing stimulation approaches.

Both single-phase materials, resulting from artificial nanostructuring, and multi-phase composites, following a mechanical coupling of the two phases, can show the simultaneous presence of ferroelectricity and ferromagnetism. Between them, the composites are preferred thanks to their superior magnetoelectric parameters at room temperature [12, 13]. Depending on the material composition, it is possible to distinguish between different types of MENPs, which properties differ by changing the dimension, the structure, the materials, and the frequency of the magnetic fields used to elicit the magneto-electric effect [12, 13]. Fig.1 shows some examples of connectivity, such as spherical core-shell nanoparticles with a ferromagnetic core and a ferroelectric shell, concentric magnetic/piezoelectric tubes, composite of piezoelectric ceramics or piezopolymers with embedded magnetic nanoparticles or magnetic rods, particulate composite with ferromagnetic and piezoelectric particles embedded in a neutral matrix and composite in a planar heterostructure containing two or more alternating ferromagnetic and piezoelectric layers [12, 13]. Among all, the core-shell cobalt ferrite ($CoFe_2O_4$) barium titanate ($BaTiO_3$) nanoparticles represent the most widely used type of MENPs [12–17].

In MENPs, the strain-induced lattice match between the two magnetostrictive and piezoelectric components allows the conversion of magnetic to electric energy or vice versa. In fact, when influenced by a magnetic field $\mathbf{H}$, the ferromagnetic phase deforms due to magnetostriction. Then, through the interface between the two ferroic phases, the deformation is transferred to the ferroelectric one, which changes polarization $\Delta\mathbf{P}$ and in turn, the electric field $\Delta\mathbf{E}$, due to the piezoelectric effect. This is known as the direct effect. Conversely, the converse effect determines a change in the magnetization $\mathbf{M}$ of the MENP under the action of an external electric field $\mathbf{E}$. What characterizes the magnitude of the linear ME effect in the material is the magnetoelectric coefficient α,

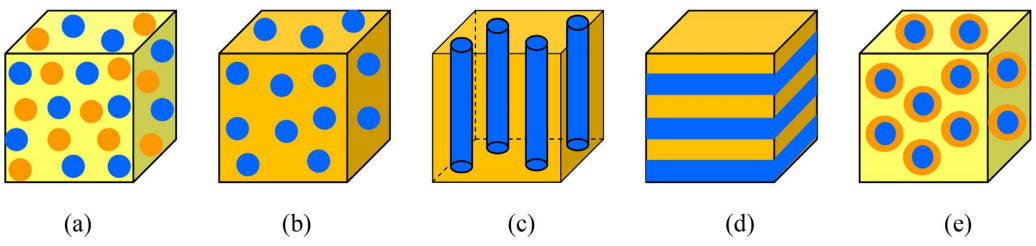

Figure 1: Composite ME materials of various types of connectivity: (a) FM and PE particles embedded in a neutral matrix; (b) FM particles located in a PE matrix.; (c) FM rods in a PE matrix; (d) Planar heterostructure containing two or more alternating FM and PE layers; (e) - core-shell nanoparticles. Highlighted in color: yellow - dielectric matrix; orange - piezoelectric PE; blue - ferromagnet FM. Taken from [12].

defined as the ratio of the polarization change following a change of the magnetic field $\alpha = \Delta\mathbf{P}/\Delta\mathbf{H}$ [V/cmOe], or alternatively, as $\alpha_E = \Delta\mathbf{E}/\Delta\mathbf{H}$ [V/cmOe] [12–14]. MENPs can be either placed in the target region (e.g. by stereotactic injection in a specific brain region [15]) or introduced in the body, by e.g. intravenous injection, and then driven to the target region via the application of a magnetic field gradient [18]. Finally, through the application of a proper a.c. magnetic field at a specific low frequency, MENPs can be activated [13, 14]. Post-treatment, by applying a reversed magnetic field gradient, MENPs can be pulled away from the localized area. However, it is noteworthy that nanoparticles are excreted from the body within a two-month period, depending on their size and on the particular organ in which they are, as shown in a mouse model [19].

MENPs have displayed an entirely new set of unique applications thanks to the strong coupling of local intrinsic electric fields at the intracellular level with external magnetic fields, enabling wireless control of cellular processes in any organ. Some examples of functions that have currently implied MENPs are in vitro applications such as magnetic tweezers and magnetic separation of proteins and DNA molecules, drug delivery, nano-electroporation, and brain stimulation, as described in [12], [14], [16] and [15]. More specifically, [12] and [15] have evidenced the activation of neural pathways following brain stimulation with MENPs. When stimulated with a low-intensity magnetic field, MENPs generate a.c. signals at the same frequency as the activity of a healthy nerve charge. The vibration of a ME nanoparticle leads to the activation of neurons around it with the same frequency, that is, to their stimulation non-invasively.

Due to their potentiality, MENPs could be possibly integrated as innovative tools based on electromagnetic fields for the development of bio-hybrid interfaces providing interconnection between living and artificial systems. The emerging nanotechnologies will allow further improve the maximization of the efficacy of wireless stimulation, thus developing new strategies for stimulating and sensing peripheral and central nervous systems, and opening up unprecedented possibilities for biomedical applications.

To provide significant insights into the design of neuroprosthetic devices, and reduce the translational time needed for in-vitro and in-vivo validation, computational modeling is particularly valuable. The computational approach allows the efficacy assessment and the evaluation of treatment and device safety, powering the optimization of the medical device performance and boosting the translation of the wireless stimulation with MENPs in the clinic. The coupling of EM-neuronal dynamics is required when studying stimulation thresholds, the impact of pulse shape, and the selectivity of activation inside the neuronal fibers; the distribution of the inhomogeneous electric field in the human body, and the complex interplay between the two. Hybrid models (HMs), given by a combination of finite element method FEM and computational solver for neural response determination, together with computable phantoms are the fundamental tools in computational neuroengineering [20]. Both simplified models or more realistic volumes, such as human phantoms [21] or region-specific human [4] models, can be used in the simulations, varying the level of detail and so the complexity of the model. Human phantoms or region-specific human models are downloadable from IT'IS foundation. More in detail, virtual population models are a set of highly detailed virtual human models, generated from magnetic resonance image data of volunteers, empowered with integrated multi-physics solvers, tissue models, and functions such as posing and morphing. Each model distinguishes over 300 different tissues and organs for which dielectric and thermal properties are available [21]. Regional human models are instead models of specific organs or regions of the body developed on high-resolution multimodal imaging data. They make available ultra-high resolution models for specific organs. Examples can be the MIDA model [22], an ultra-high resolution head and neck model, or the Ella right-hand model [23].

The aim of this work is to prove the feasibility of using MENPs as tools for the next generation of bionic interfaces for human arms, by investigating their potential for the electric stimulation of peripheral nerves. Computational approaches were used to simulate direct nerve stimulation, playing a pivotal role in the evaluation of electric quantities within human tissues and investigating the physical phenomenon behind the stimulation effect. In this article, all the simulation settings for the computational approach are reported, and the results are presented and discussed. This research is in the framework of one of the ongoing projects "Fit4MedRob- Fit for Medical Robotics" Grant (contract number CUP B53C22006960001) financed by the Italian Ministry of Research (MUR) under the complementary actions to the NRRP (PNC0000007).

2. Material and Methods

The methodology used to assess the feasibility of using MENPs for the stimulation of peripheral nerves, in this study, consists of two phases, as described by the flowchart in Fig.2. At first, the simulations presented a very simple framework, with a single nanoparticle and a single motor neuron with a simplified geometry, into a cylindrical environment emulating the surrounding environment of the nerve. Here, the dynamic response of the neuron to the stimulus delivered by the MENP has been analyzed. Both the influence of the MENP-neuron distance and the impact of using different stimulus pulses were investigated. As a second step, a more detailed model, accounting for the realistic anatomy of a peripheral nerve, was used to assess the feasibility of using single and multiple MENPs for achieving neural stimulation. A conclusive paragraph will describe the metrics used for the analysis.

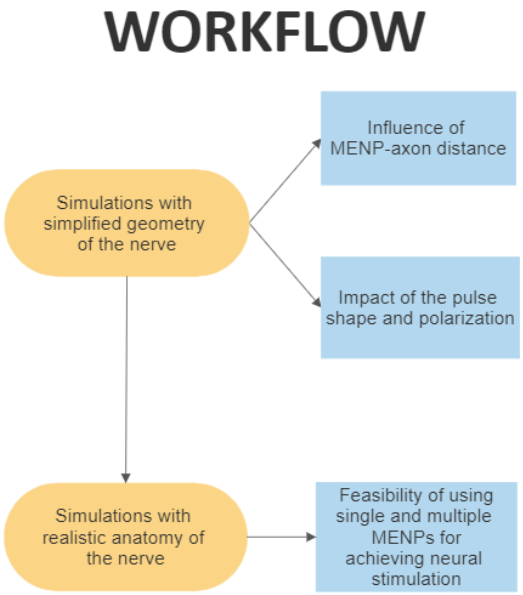

Figure 2: Flowchart illustrating the workflow of the present study.

Both the analysis of the simplified geometry neuron and the anatomical detailed peripheral nerve were implemented by two different steps, as foreseen in hybrid models. The first one involves the resolution of the electric field distribution **E** elicited by the MENP in the biological structure, while the second one consists of the neural response determination by the dynamics model of nerve behavior.

All the simulations have been implemented using the Sim4life platform (by ZMT Zurich Med Tech AG, Zurich, Switzerland, www.zurichmedtech.com). Hereafter, all the steps are reported more in detail.

2.1. Simulations on motor nerve with simplified geometry

In this section, all the simulations that have been run to study the interaction between a single MENP and a single fiber are summarized. At first, the MENP model and electromagnetic stimulation settings are described. Then, the model of the nerve dynamics is reported. Finally, all the simulation settings of the different simulations are illustrated.

The results of these simulations were analyzed in terms of:

- the influence of the MENP - fiber distance over the response of the neuron;
- the strength-duration (SD) curve, and the comparison of the SD with different pulses;
- the relevance of the MENP's stimulus polarization pulse on the neuron's action potential.

2.1.1 Electromagnetic stimulation settings and MENP model

When stimulated with a low-amplitude magnetic field, thanks to its magneto-electric effect, MENP exhibits an electric potential on its surface with dipolar distribution aligned along the direction of the stimulating magnetic field. Accordingly, in this study, the magneto-electric effect was modeled by approximating the MENP

geometric structure of a sphere with two conductive surfaces separated by an insulating layer, as shown in Fig.3.

Considering the wide range of dimensions of the MENPs reported in the literature, which varies between 30 and 600 nm, [13], [15], [24], [25], depending on the synthesizing method used, in this study a spherical MENP with a diameter equal to 80 nm was modeled.

In typically implanted bipolar electrodes configuration, a potential of +/-0.5 V is set to the electrodes [26]. To favor the comparison between MENPs and traditional electrodes-based stimulation and for the sake of scalability, here a potential of +/- 0.5 V has been assigned over the two MENP surfaces by using Dirichlet boundary conditions, with a total charge of 1 V. Moreover, this value sounds reasonable considering magneto-electric coefficient values described in the literature [27]. The insulating layer was of techotane material, with dielectric properties assigned according to literature data [28] at the MENP stimulating frequency.

The ohmic quasi-static approximation was adopted to solve the low-frequency electromagnetic problem. It is one of the FEM numerical methods for solving partial differential equations in complex geometries when the analytic method would be cumbersome. Some implicit assumptions hold in the simulations when the FEM ohmic quasi-static approximation is used. They are the following:

- The membrane potential varies only longitudinally with respect to the fiber course, so the transverse excitation is neglected;
- The fiber excitation does not affect the electric potential in the surrounding area.
- All the media are purely resistive, and thus capacitive phenomena can be neglected [4, 20], all changes in current affect the potentials of the entire space immediately.

Through FEM, the Laplace equation used to obtain the electric potential (ϕ) became:

$$\nabla \cdot (\sigma \nabla \phi) = 0 \tag{1}$$

where σ (S/m) is the electrical conductivity of tissues set according to the stimulating frequency. Then, the **E** field distribution was derived by means of the following relation:

$$\mathbf{E} = -\nabla \phi \tag{2}$$

The frequency of the electromagnetic stimulation problem was set to 100 Hz, which is in the frequency range for neural stimulation, as reported in literature [16]. Dirichlet boundary conditions with $V = 0$ defined the potential on the borders of the computational domain. The estimation of the electric field **E** distribution elicited by the MENP localized in biological tissue is the estimated output of the FEM method and the input of the neural simulation described in the next section.

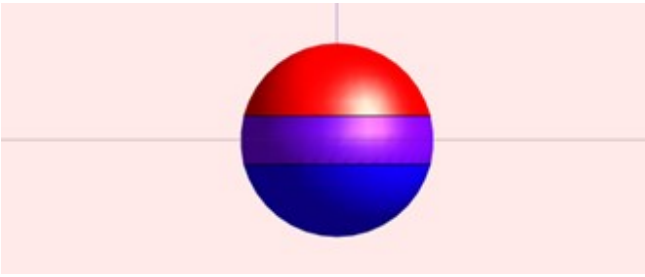

Figure 3: MENP model in Sim4life. Red shell with V=0.5 V, Blue shell with V=-0.5 V, and middle layer in purple with techotane material

2.1.2 Nerve model and titration factor

The system under investigation consisted of a cylindrical structure, of 1000 um length and 100 um width, and a single neuronal fiber, of 1000 um length and diameter equal to 5.7 um.

The computational solver used to determine the effects of the electric field generated on the neural structures is NEURON (https://neuron.yale.edu/neuron/). NEURON is a powerful environment for the implementation of biologically realistic models about the electrical and chemical signaling in single neurons and a small network of neurons. It simulates the equations that describe the nerve cells, the so-called cable equations, and solves them computationally. Its aims are both to test hypotheses about the mechanisms that govern the signaling and simulate efficiently the before mentioned chemical and electrical mechanisms. NEURON environment does not

allow an infinitely detailed biological realism, but its choice is at the discretion of who constructs the model, giving the possibility of creating a new model of transmembrane dynamics or using one of the already existing ones.

To better identify the most suitable model to use in this research, an investigation of the models describing differently the time response of a neuronal membrane to external potential fields was necessary.

Spatially Extended Nonlinear Node (SENN), MOTOR (MRG), Modified MRG Models, Small fiber modified MRG Models, RAT, SWEENEY, and Unmyelinated Sundt C-fiber models are available in NEURON to describe the transmembrane dynamics. Among all of them, the small fiber-modified MRG model, the RAT model, and the unmyelinated Sundt C-fiber have been excluded from the literature analysis because they characterize the membrane dynamics of fibers which are out of the scope of peripheral nerve stimulation. The chosen models are briefly presented in the following.

The Spatially Extended Non-linear Node (SENN) model is a single cable model for extracellular stimulation of a myelinated nerve axon [29, 30]. It is based on studies of frogs, and the body temperature is 20°C [30].

The SWEENEY model is a single cable model of myelinated nerve based on the properties of mammalian myelinated nerve. This model is based on the study of rabbits, and it was developed to overcome the limitations of the models based on Frankenhaeuser and Huxley equations, which rely on the study of amphibians [31].

The MOTOR (MRG) model is a computer-based double cable model of mammalian nerve fibers modeling the recovery cycle, so the threshold fluctuations after a single action potential [32]. It is based on studies of humans, cats, and rats, and the body temperature is 37°C [30]. The MOTOR model has been highlighted as the most representative of the nerve behavior in human arms, which is the application of interest for this study. Its modeling based on human nerves enables it to properly approximate the electric response of a peripheral nerve localized near the MENP.

In the end, the modified MOTOR models describe the membrane dynamics of myelinated sensory and motor axon fibers. The two different models are built by including the electro-physiological differences between the two axons in the double-layer MRG model. Membrane properties derived from physiological data and/or validated in prior modeling studies were useful for this purpose [33].

In this study, the MOTOR model was chosen to simulate the neuronal dynamic of the neural fiber. Its equivalent circuit, in Fig.4, consists of explicit representations of the nodes of Ranvier, paranodal and internodal sections of the axon, and a finite impedance myelin sheath. Both linear and nonlinear membrane dynamics are used to model the electrical behavior of the axon and the coexistence of two different layers at the internodal compartments characterizes its double cable structure. Particularly, the nodes are a parallel combination of nonlinear fast Na, persistent Na, slow K conductances, linear leakage conductance, and membrane capacitance. Whereas the internodes comprise paranodal and internodal compartments, representing the myelin sheath and underlying axolemma respectively. In the circuit, both of them include a linear conductance in parallel with the membrane capacitance [32]. The dynamics of the model are described by motor equations in all the nodes of Ranvier [30]. Since little data exists describing the membrane dynamics of the channels, the parameters associated with the kinetics were selected on the base of enabling the model to reproduce a wide range of experimental data [32].

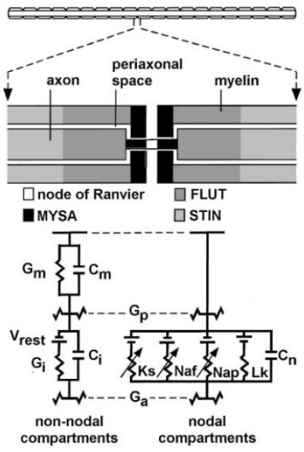

Figure 4: Equivalent circuit model for excitable membranes in MRG model. Taken from [32].

The neuronal dynamics solver NEURON, developed as a library in Sim4life software, allows the implementation of the titration mechanism in the simulations. Titration consists of stimulating the axon varying the amplitude of the stimuli to identify the threshold above which the axon is depolarized. The equation used to find the final threshold current is $I_T(t) = I * T * a(t)$, where I is the current from the EM field, $a(t)$ is the modulating pulse and T is the titration factor. The current and the modulating pulse are defined in the simulation settings, whereas the titration factor is varied until a response is detected [26]. This factor is important to estimate the minimum pulse amplitude able to elicit an action potential. The titration factor was implemented in all the simulations of this case study.

2.1.3 Stimulation Settings

To separately investigate the influences of the distance and the stimulus pulse shape, more simulations with different settings have been run. The pulse used to stimulate the nerve differed in the simulations, but it had always duration and time step equal to 200 ms and 0.0025 ms, respectively.

First of all, the importance of the MENP-fiber distance was explored. The pulse was a sinusoid of one period with an amplitude equal to the one obtained by the electromagnetic simulation and a frequency equal to 100 Hz. The tissue of the cylinder was nerve, with electric properties assigned according to literature data [28] at the MENP stimulating frequency. MENP was placed at different distances from the line representing the nerve, equals to 0.5 um, 1.3 um, 2 um, 3.5 um, 5 um, 10 um, 20 um, and 30 um.

Then, the strength-duration curve was studied, and a comparison of the neuron response over a sinusoidal or bipolar stimulus was accomplished. The MENP-fiber distance was 0.5 um, and the material of the cylinder was nerve, from [28] at the MENP stimulating frequency. The stimulus shape varied: both a one-period sinusoid and a single bipolar pulse have been considered. Their amplitude was the one obtained by the electromagnetic simulation, so the titration factor. The stimulus frequencies compared for the SD curves ranges from 10 to 1000 Hz.

In the end, the relevance of the MENP's stimulus polarization on the neuron's action potential was investigated. The tissue was nerve from [28] at the MENP stimulating frequency, and the distance was 0.5 um. The stimulus was a sinusoid, with a 100 Hz frequency and amplitude equal to the titration factor. Both polarizations were investigated in the simulations.

2.2. Simulations on motor nerve with realistic geometry

After the study of the behavior of the neural fiber in different stimulation settings, the investigation of the influence of MENPs over the fibers of a human arm continued through simulations in a more realistic environment.

2.2.1 Electromagnetic stimulation settings and MENP model

The electromagnetic stimulation settings and the MENP model were unchanged.

2.2.2 Nerve model

The nerve model was more complex and, more precisely, the nerve was represented by a realistic cylindrical model in a saline solution, as shown in Fig.5. The use of the saline solution as the external medium was necessary to both simulate zero potential at infinity and to approximate the intraoperative extra neural space [4]. Some assumptions and simplifications concern the model [4, 34]:

- Properties such as diameter, myelination, and channel densities stayed constant along the axon length;
- Layers of tissue surrounding the fascicles and nerves were modeled with a circular symmetry and the same material. The material was nerve from [28] at the stimulating frequency.
- The intraneural displacement of the fibers, so their tortuosity, is not represented.
- The fibers in all the fascicles were the same. The model of the neuron was the MRG model and the fibers had the same diameter of 5.7 um.

In the model, it is possible to distinguish the saline solution, the nerve, the interstitial layer, three different connective tissues, three different blood vessels, and seven fascicles of fibers. The dielectric properties are assigned according to literature data [28] at the MENP stimulating frequency. In Fig. 5b, the fascicles of fibers are clearly visible and numbered to be differentiated.

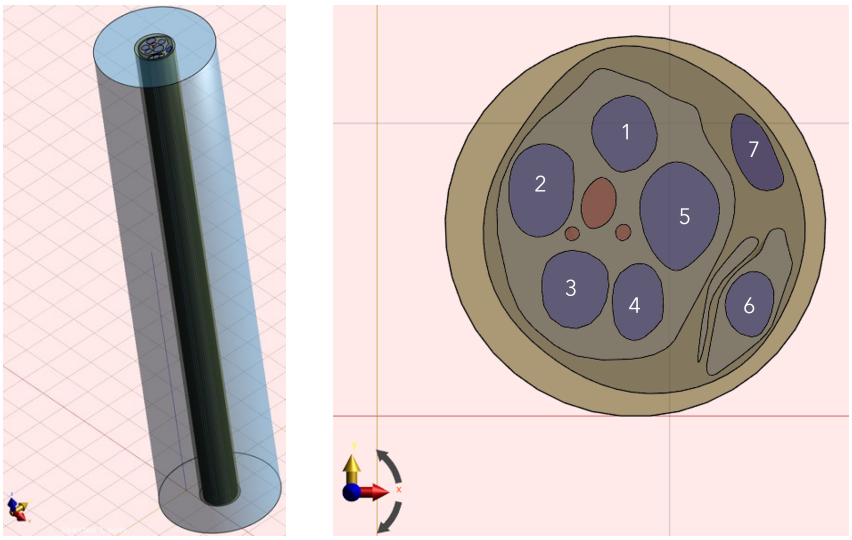

(a) Camera view of the model.

(b) Lateral view of the model.

Figure 5: Realistic model of the nerve

2.2.3 Stimulation settings

The same stimulus pulse was run in all the simulations. It was a sinusoid of one period, with an amplitude equal to the one obtained by the electromagnetic simulation, a frequency of 100 Hz, and duration and time step equal to 200 ms and 0.0025 ms, respectively.

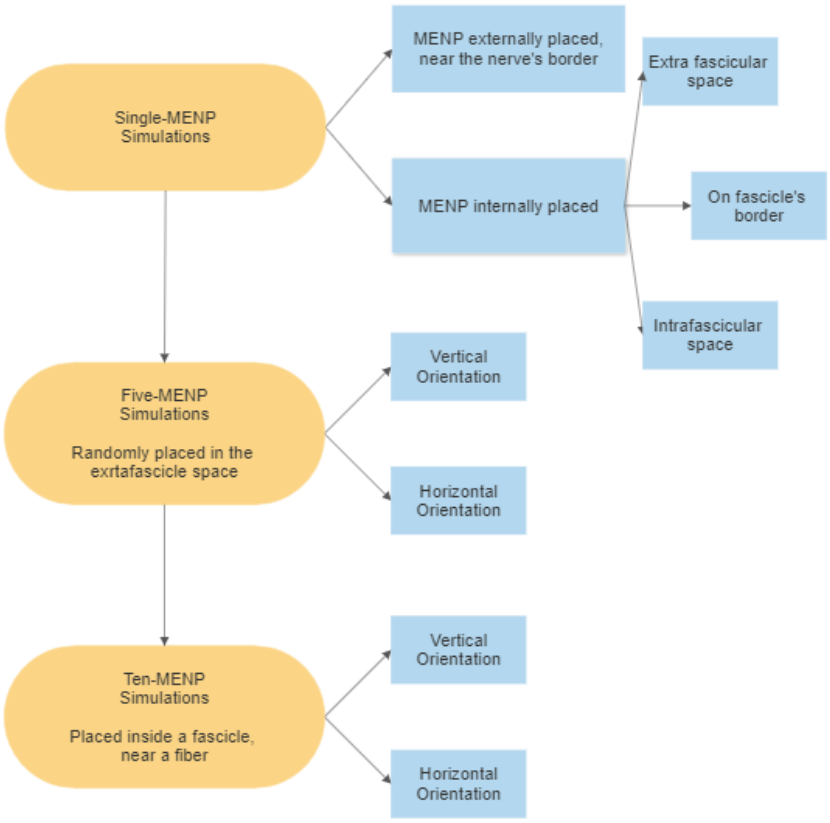

Figure 6: Flowchart illustrating the workflow of the realistic model simulations.

Some case studies differing on the number of MENPs and their configurations were analyzed. The workflow is shown in Fig.6. Initially, the influence of a single MENP over the realistic model was analyzed. The MENP was first placed on the border of the nerve, and then inside it. Internally the nerve, the MENP was placed externally, on the border, or inside the fascicles. The height of the MENP along the nerve varied. A total of seven distinct simulations have been run. Then, two different simulations with five nanoparticles each were run. The MENPs were randomly placed in the extra-fascicular space, arranged in a line along the fiber length with an inter-distance of 0.5 um, Figs. 7a. The MENPs were differently oriented in the two configurations, Fig.7b. Last, the influence of ten MENPs over the fiber response was studied. Two different simulations were run. The MENPs were placed inside a fascicle, near a fiber. They were arranged in five couples aligned along the fiber length. As shown in Fig.7c, the inter-distance along the direction of the fiber was 0.5 um, whereas the MENP-MENP distance perpendicular to the fiber length was 0.1 um. The MENPs were differently oriented in the two configurations, as in Fig.7b.

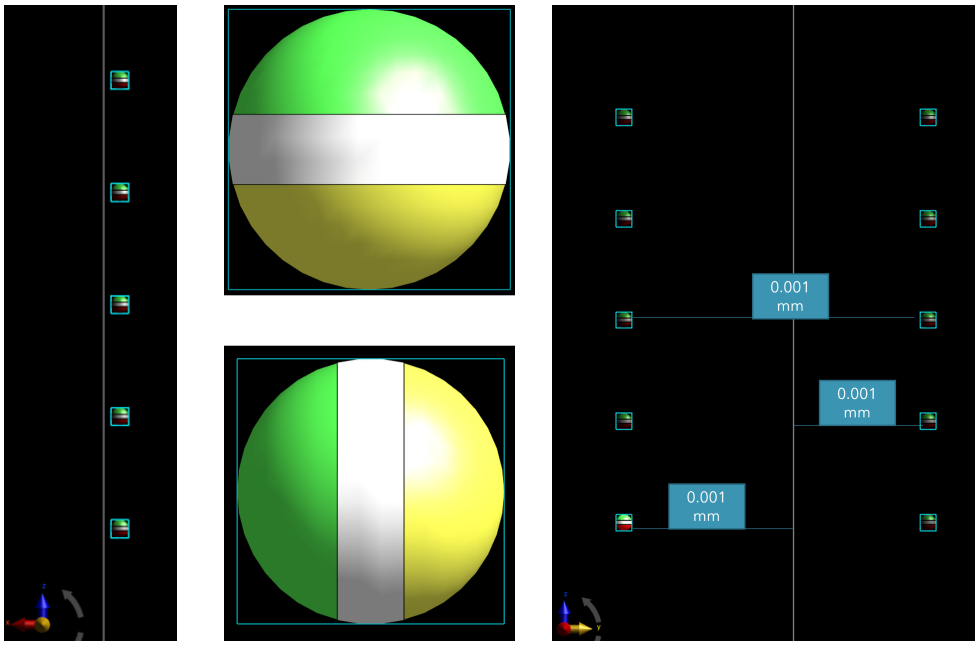

(a) (b) (c)

Figure 7: a) Zoom view of the configuration with five MENPs. b) The two orientations used in the simulations. In green and yellow are the positive and negative poles, in white the thecotane layer. c) View of the configuration with 10 MENPs.

2.3. Data Analysis

The results have been analyzed by considering different metrics. The **E** field distribution was visualized. It was decided to study the slice view with the most effective visualization of the EM distribution, which changed from case to case. Among all the possible planes, the overall field distribution was always visualized on the section holding the maximum RMS of **E** amplitude (V/m). The colormap range between 0 and 10^4 V/m was chosen as suggested by literature [14]. Moreover, the distribution of the RMS of E was studied over the neuron length. The analysis of the bell-shaped distribution was quantified in terms of width and maximum amplitude. The bell width was quantified as the length, along the nerve fiber, for which the **E** field was equal to or higher than 10% of the maximum amplitude of **E** along the same fiber. The titration factor was a useful index to estimate the stimulus amplitude of the MENP needed to elicit the action potential of the fiber. In the end, the shape of the action potential and the time of the first spike were the metrics used to investigate the neuron response.

3. Results

3.1. Simulations on motor nerve with simplified geometry

At first, the results concerning the influence of the MENP-fiber distance over the response of the neuron are reported. The analysis will be presented by considering separately the resulting electric field distribution on the nerve, the titration factor, and the neuron response for the different distances. The investigation of the distances of 5, 10, 20, and 30 nm will not be illustrated.

The **E** field distribution was studied everywhere around the MENP. Fig.8 shows the slice view over the YZ plane, which comprises the nerve along its full length. The image satisfies the requirements of the 'Data Analysis' section.

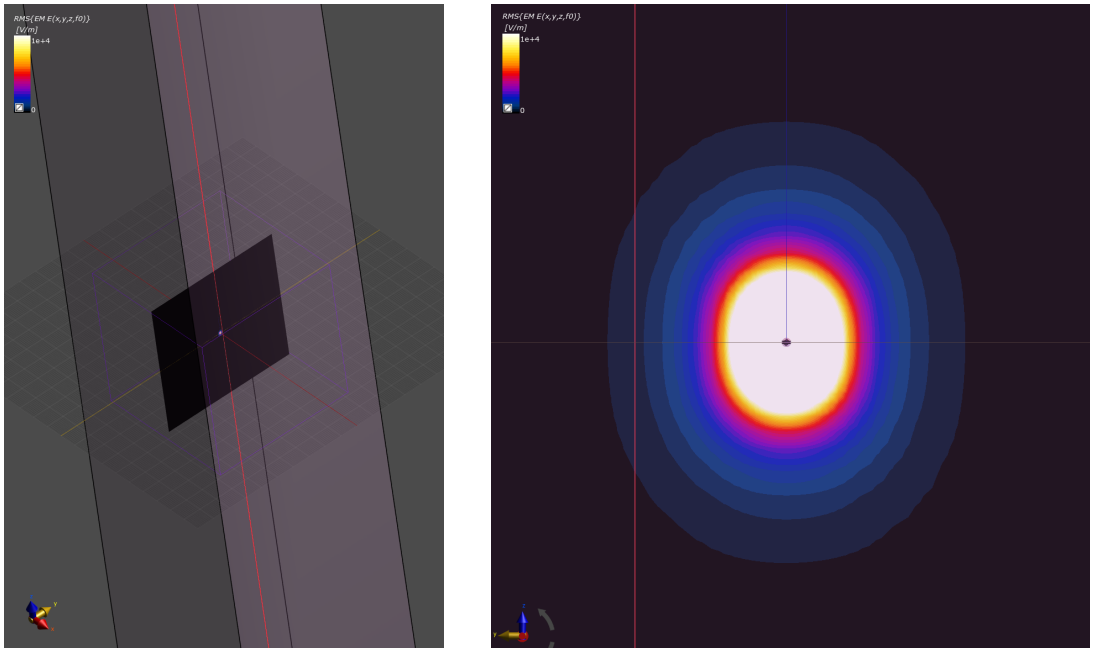

(a) Default View (b) Front View

Figure 8: View of the RMS of **E** amplitude. Visualization on the YZ plane, particularly the plan with maximum RMS **E** amplitude. The red line corresponds to the position of the neuron, and it's the line along with the **E** field is analyzed. The MENP is placed at the center of the white oval. This is the case with 1.3 um of MENP–neuron distance.

In Fig.9, the overall field of the RMS of **E** along the neuron length is reported for the MENP–neuron distances 0.5, 1.3, 2, and 3.5 um. Comparing all the results, the simulations show a similar bell shape of the distribution over the neuron length and a change in the width and the maximum amplitude of the bell. The values of the bell shape distributions are reported in Table 1 for all the distances. It was noticed that by increasing the MENP–neuron distance, the bell shape was wider and the maximum amplitude of the **E** field substantially decreased.

NP–Fiber Distance [um]	Peak Value [V/m]	10% of the maximum amplitude (um)
0.5	20929.8	1.8
1.3	466.5	7
2	157.2	9.5
3.5	30.7	14.8

Table 1: Values of the bell shape distributions.

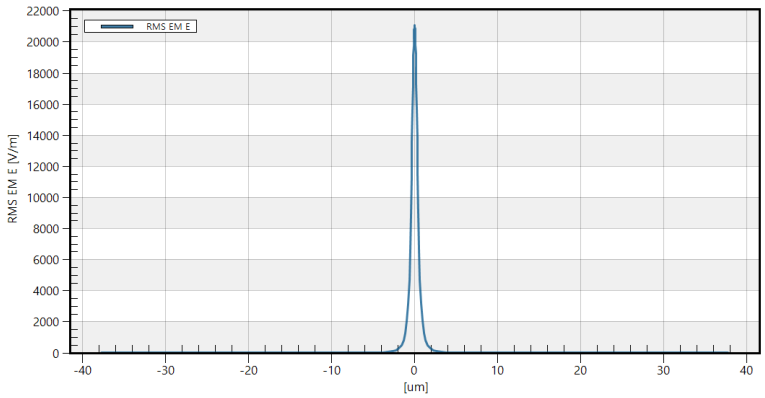

(a)

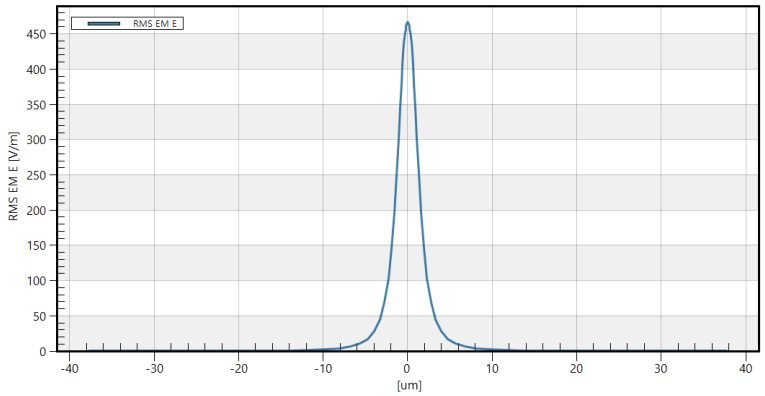

(b)

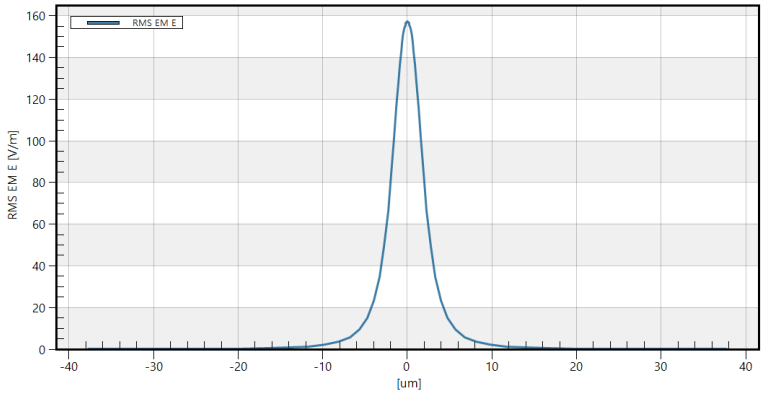

(c)

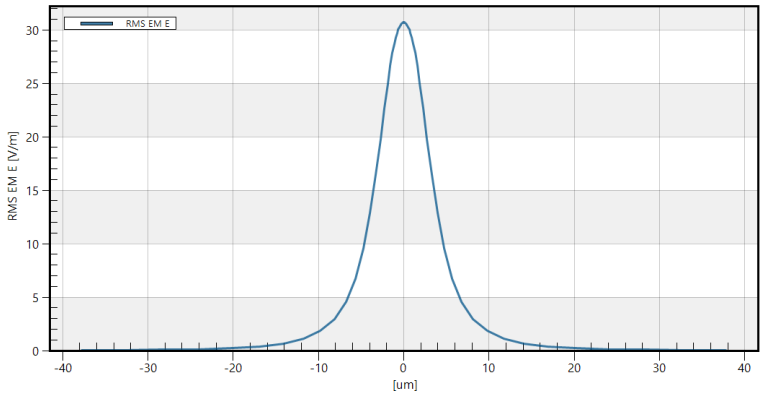

(d)

Figure 9: Overall field of the RMS of E analyzed along the neuron, for the MENP–neuron distances: a) 0.5 um, b) 1.3 um, c) 2 um, and d) 3.5 um. For the sake of readability, different scales were kept in the plots.

In Table 2, the time of the first spike in ms and the relative titration factor are presented, differentiated by the corresponding MENP–neuron distance. As well expected, increasing the distance, the titration factor increases, so a bigger stimulus amplitude is necessary to stimulate the neuron.

NP–Fiber Distance [um]	Time of first spike [ms]	Titration factor
0.5	4.38	3.16
1.3	4.44	23.25
2	4.87	74.5
3.5	4.40	362

Table 2: Comparison of first spike's time and titration factor for all the different MENP-fiber distances.

The response of the neuronal transmembrane potential has the characteristic shape of an action potential, as shown in Fig.10 for the distances of 0.5 um and 3.5 um. When considering all the different distances between MENP and the nerve, negligible differences in the shape of the action potential were observed.

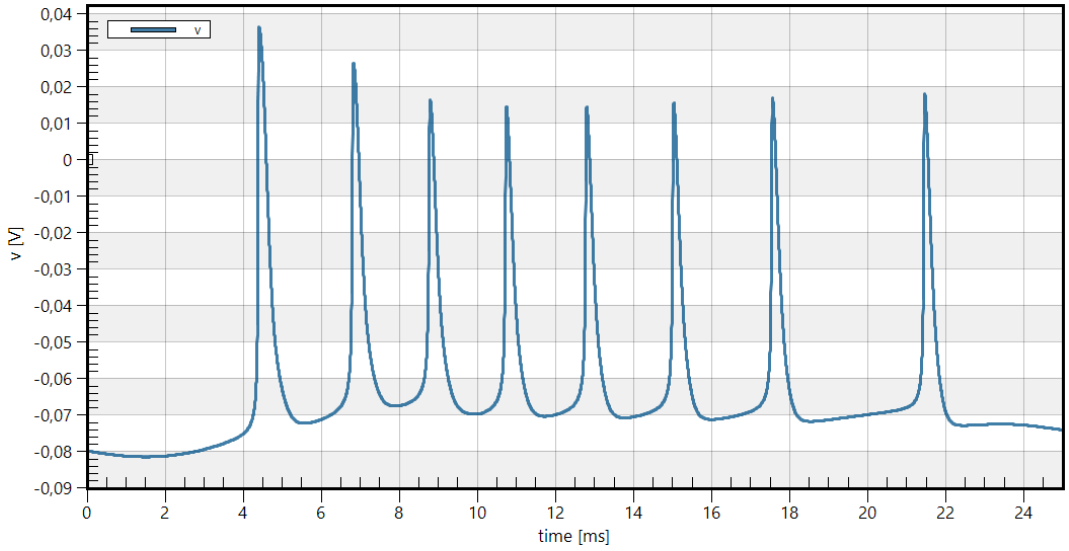

(a)

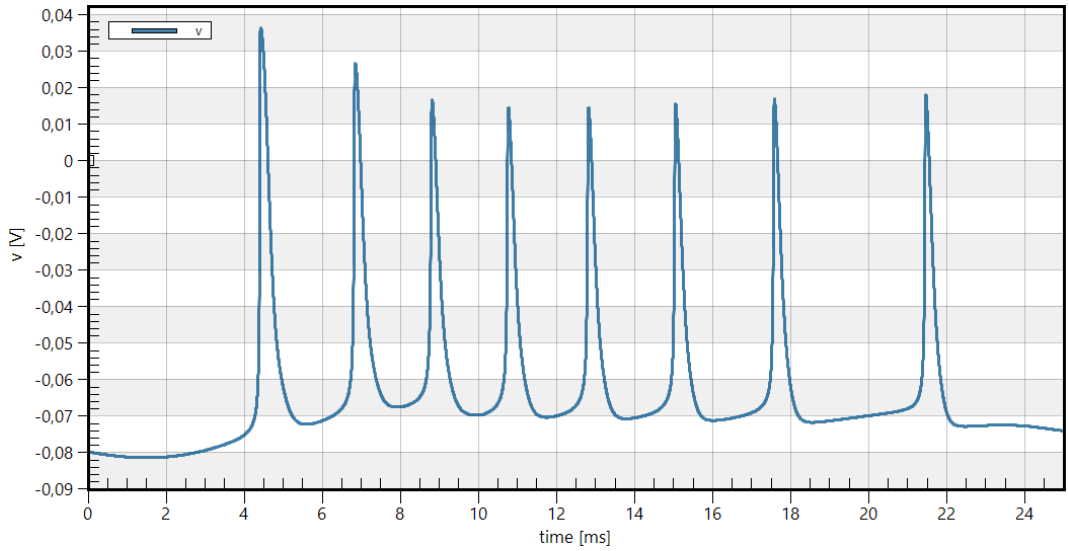

(b)

Figure 10: Nerve response, in terms of transmembrane potential (V) during the stimulation. The MENP–neuron distance varies: a) 0.5 um; b) 3.5 um.

Secondly, the strength-duration (SD) curves obtained by a one-period sinusoid and a single bipolar pulse are described. The analysis will be presented by separately showing the SD curves and a comparison of the neuronal responses varying both the stimulation frequency and the stimulus pulse.

Fig.11 presents the SD curves for the two different pulses at the MENP-neuron distance of 0.5 um, and the corresponding numerical values are reported in Table 3. The frequencies of 10, 25, 50, 75, 100, 250, 500, 750, and 1000 Hz were analyzed.

The neuronal transmembrane potential, shown in Fig.12 for the frequencies of 25 and 1000 Hz, has the characteristic shape of an action potential, which is not influenced by the pulse shape or the frequency. Differences at the beginning of the spiking time were observed in the plots. The increase in the frequency corresponds to a decrease in the time of the first spike.

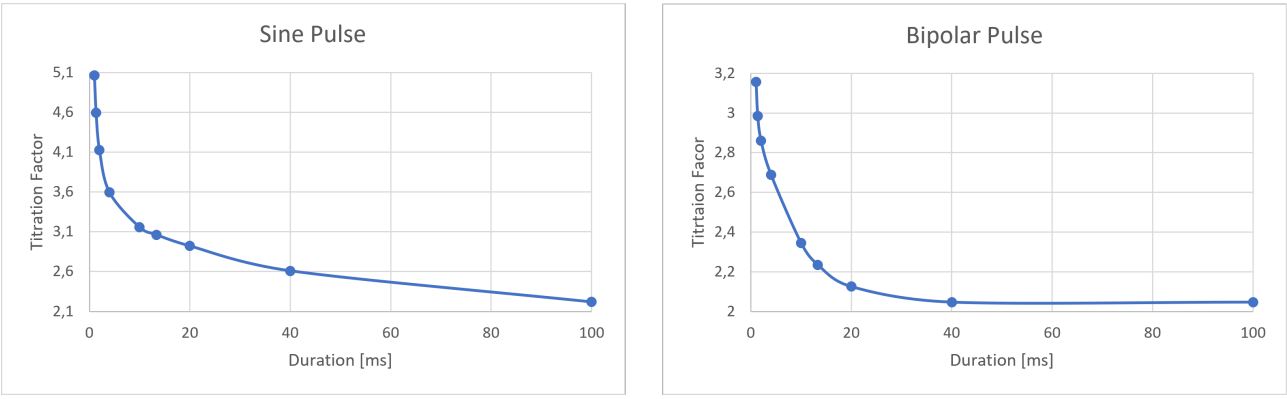

Figure 11: Strength-Duration curves comparison: on the x-axis, there is the stimulus duration in ms, and on the y-axis, there is the titration factor. The delivered pulse was sinusoidal, on the left, or bipolar, on the right. Points at frequencies of 10, 25, 50, 75, 100, 250, 500, 750, and 1000 Hz are highlighted.

Stimulus frequency [Hz]	T factor for Sine pulse	T factor for Bipolar pulse
10	2.22	2.047
25	2.61	2.047
50	2.92	2.12
75	3.06	2.23
100	3.16	2.34
250	3.59	2.69
500	4.12	2.86
750	4.59	2.98
1000	5.06	3.16

Table 3: Comparison of the titration factors of the two different pulses for the same stimulating frequency.

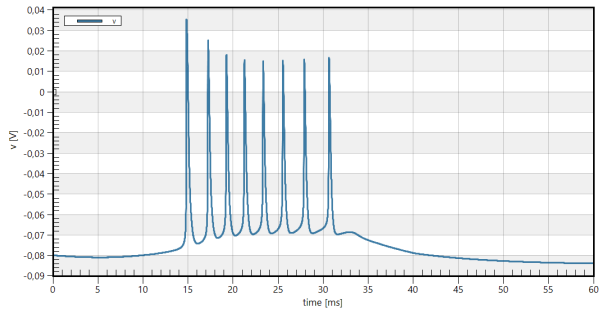

(a) Sine pulse, 25 Hz.

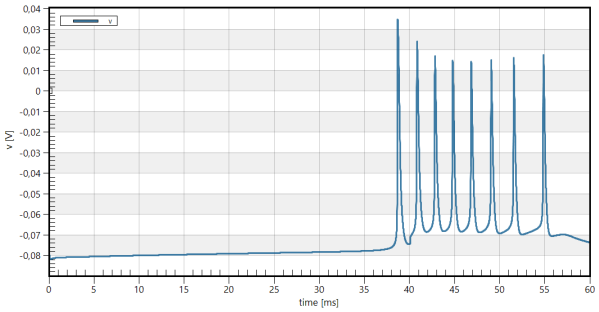

(b) Bipolar pulse, 25 Hz.

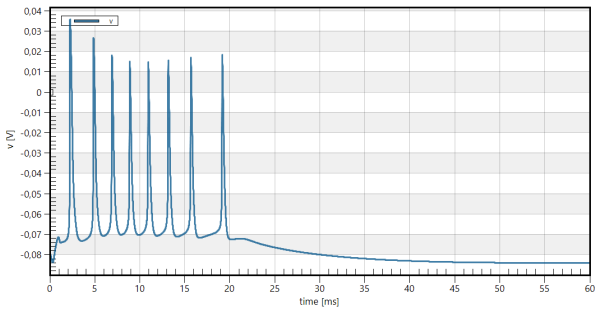

(c) Sine pulse, 1000 Hz.

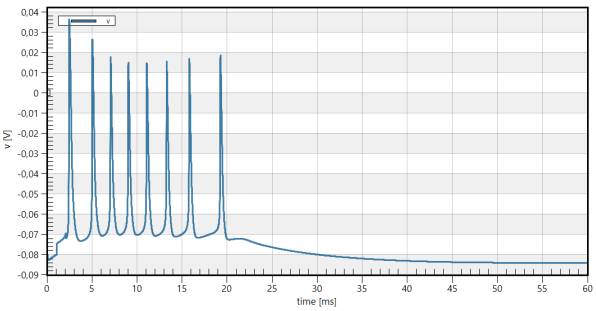

(d) Bipolar pulse, 1000 Hz.

Figure 12: A comparison of the neuron response varying the stimulus pulse and the frequency.

At last, results highlighting the relevance of the MENP's stimulus pulse polarization on the neuron's action potential are illustrated. The analysis presents the titration factor and the neuron response.

Table 4 summarizes all the titration factors necessary to elicit the neuron's response and the time of the first spike in ms for the two polarizations for each distance. For both polarizations, the stimulus amplitude needed to stimulate the neuron increases by increasing the MENP-neuron distance. As well expected, the inverse polarization increases the time interval before the start of the spiking activity and decreases the titration factor needed compared with the values in the direct polarization.

The neuron response has the characteristic shape of an action potential, as in Figs. 10 and 12. The spiking activity has negligible variations between the simulations, changes in the responses were due to the different first spike times.

	Direct Polarization		**Inverse Polarization**	
NP–Fiber Distance [um]	**Time of first spike [ms]**	**Titration factor**	**Time of first spike [ms]**	**Titration factor**
0.5	4.38	3.16	9.34	3.01
1.3	4.44	23.25	9.27	22.25
2	4.87	74.50	9.24	71.50
3.5	4.40	362	9.37	346

Table 4: Comparison of first spike's time and titration factor for the distances.

3.2. Realistic simulations

The analysis will be presented in terms of electric field distribution on the nerve, titration factor, and neuron response, as exposed in 'Data Analysis'. For the sake of clarity, the results highlighted as the most significant among the case studies will be reported. The simulations with a number of one, five, or ten MENPs will be considered separately.

At first, a comparison of the results with a single MENP and variable positioning will be presented. Four out of seven simulations have been chosen as the most meaningful to report. More in detail, a case study per configuration will be illustrated. The highlighted results refer to the MENP placed near the border of the nerve, extra fascicular in the space between fascicles 1 and 5, on the border of fascicle 5, and in the intrafascicular space of fascicle 4. The **E** field distribution has been displayed over all the planes, and the most effective visualization is on the XY plane. Varying the MENP position, negligible differences among field distributions were observed, except for the simulation with the MENP placed on the border of a fascicle. A juxtaposition is shown in Fig.13.

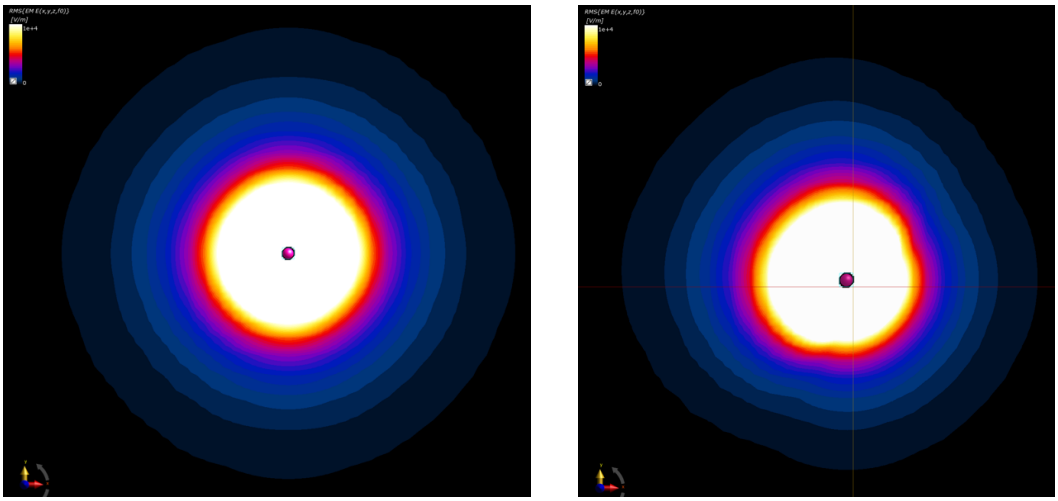

(a) (b)

Figure 13: **E** field distribution on the XY plane. a) In the simulations, the MENP was placed on the border of the nerve, extra fascicular, or intrafascicular; b) the MENP was on the border of a fascicle.

The titration factor needed to elicit the action potential was investigated for every neuronal fiber of the seven fascicles. In Table 5, the titration value and the time of the first spike in ms of three different neurons belonging to three different fascicles are compared. The reported values refer to the fiber number 3 in fascicles 1, 4, and 5. The time of the first spike is not subjected to variations influenced by the changing position of the MENP. The titration factor is instead altered. As expected, the biggest values refer to the MENP positioned on the border of the MENP, and the lowest to intrafascicular simulation. Higher intensity is needed when the MENP is placed on the border of the fascicle than when the MENP is placed extrafascicular.

MENP location	**Time of first spike [ms]**			**Titration factor**		
Nerve's border	4	4	4	$1.15*10^6$	$1.1*10^7$	$3.67*10^6$
Extra fascicular	4	4	4	491520	$2.74*10^6$	382976
Fascicle's border	4	4	4	892928	$2.08*10^6$	475136
Intrafascicle	4	4	4	860160	47872	313344

Table 5: Comparison of first spike's time and titration factor for three different neuronal fibers belonging to fascicles 1, 4, and 5, respectively. The location of the MENP varied in the four simulations.

Then, the results of the configuration with five MENPs are reported, and the two orientations are compared. The most effective visualization for the **E** field distribution has been found to be on the XZ plane. The vicinity of the MENPs causes an overlap of the **E** fields, and the different MENPs' orientation varies the distribution in the two cases, as clearly visible in Fig.14.

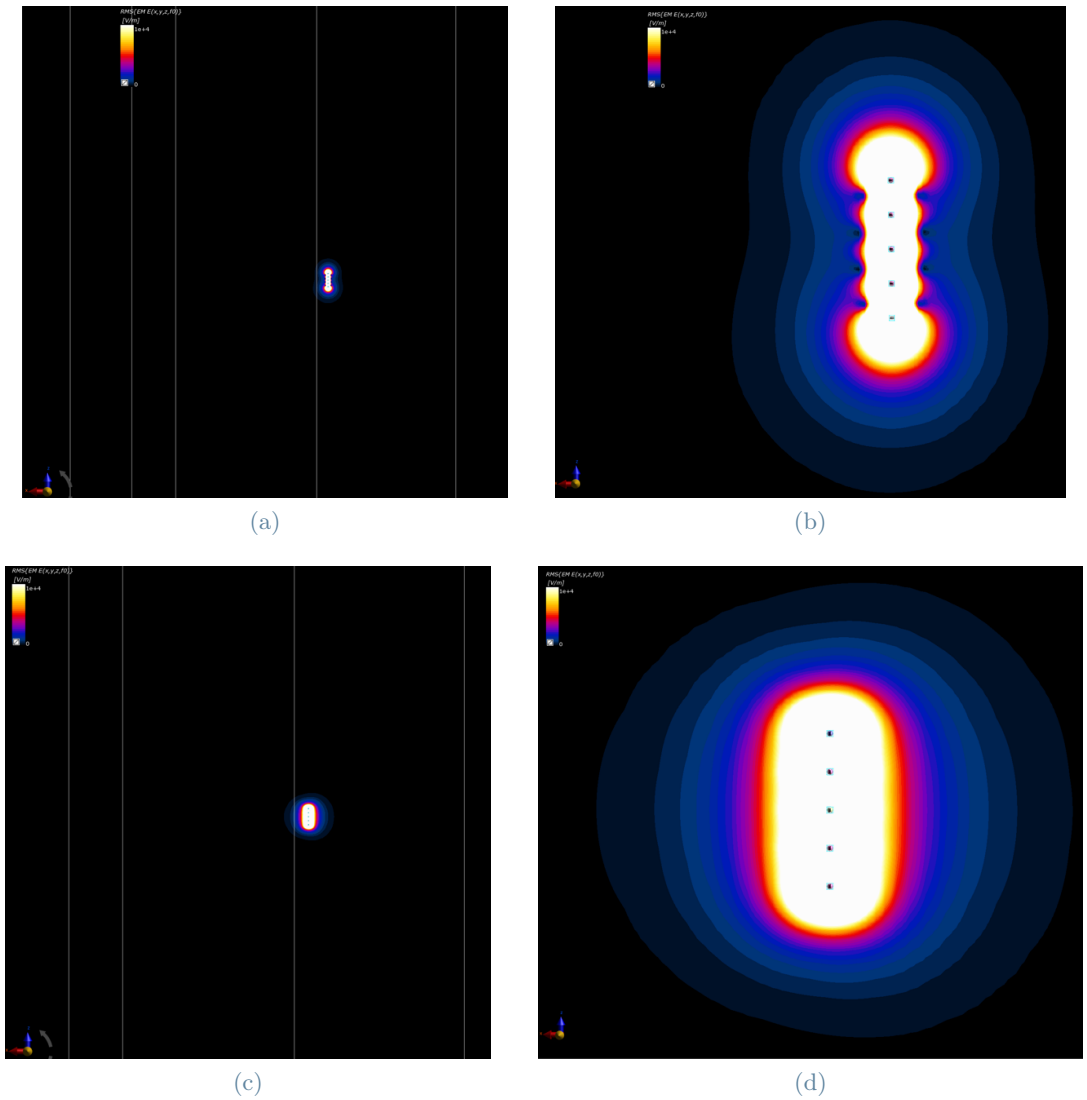

Figure 14: **E** field distribution on the XZ plane. a) Far and b) Zoom views in the configuration with 5 MENPs orientated as in Fig. 7b top. c) Far and d) Zoom views in the configuration with 5 MENPs orientated as in Fig. 7b bottom.

The titration factors needed to activate the neuronal fibers are differentiated in Table 6. The investigation was for every neuron of the seven fascicles, but the results presented in this work will refer to fiber number 1 in fascicles 3 and 4, and fiber number 3 in fascicle 2. The five MENPs were placed in the extra fascicular space between fascicles 3 and 4, and ideally, the first two neuronal fibers are the nearest to the stimulating point, and the last one is the furthest. The results concerning both the vertical orientation of the MENPs, Fig.7b top, and the horizontal one, Fig.7b bottom, will be shown. The titration factors are generally higher in the horizontal configuration, and the location of the first spike, not reported here, varies by changing the MENPs orientations. As expected, lower stimulus amplitudes are needed for neurons placed nearer to the MENPs.

MENPs orientation	**Time of first spike [ms]**			**Titration factor**		
Vertical	3.16	2.96	3.63	212992	14592	10816
Horizontal	4	4	4	$1.6*10^6$	66048	108544

Table 6: Comparison of first spike's time and titration factor for three different fibers. Neuronal fibers are number 3 in fascicle 2 and fiber number 1 in fascicles 3 and 4, respectively. The orientation of the MENP varied in the two simulations.

In the end, the results of the configurations with ten MENPs. Among all the possible visualizations of the **E** field distribution, the most effective one was on the YZ plane. The **E** field distribution is visible in Figs.15a and 15b for both configurations. As for the case of five MENPs, the **E** field distribution is influenced by the vicinity of the MENPs, and their fields are overlapped. Figs. 16a and 16b show the overall field of the RMS of **E** along the neuron length for both configurations. The width of the bell-shaped distribution decreases, imitating an impulse shape. The peak amplitude changes in the configurations: values slightly over 3500 V/m and 16000 V/m correspond to the vertical orientation and the horizontal one, respectively.

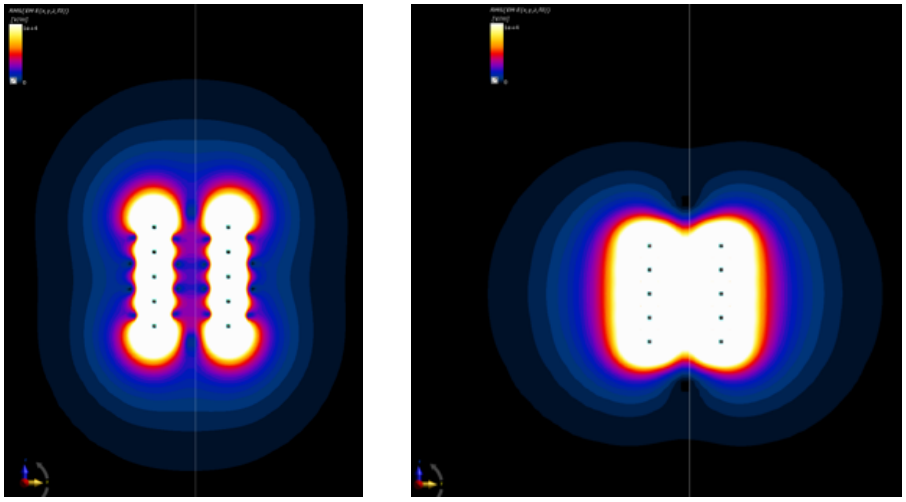

(a) (b)

Figure 15: View of the RMS of **E** distribution on the YZ plane, particularly the section with maximum RMS, and of the RMS of **E** plot analyzed along the neuron length. a) Zoom view of the RMS of **E** distribution in the configuration with 10 MENPs orientated vertically, as in Fig. 7b top. b) Zoom view of the RMS of **E** distribution in the configuration with 10 MENPs orientated horizontally, as in Fig. 7b bottom.

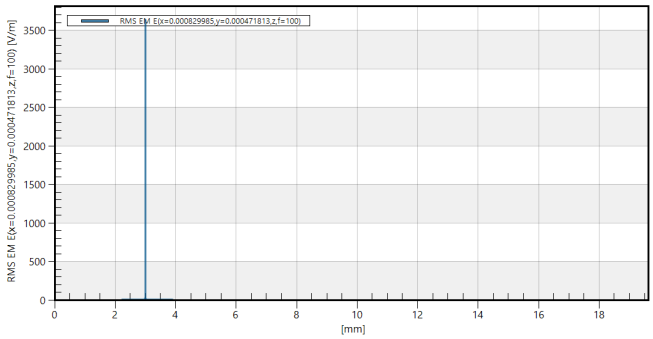

(a)

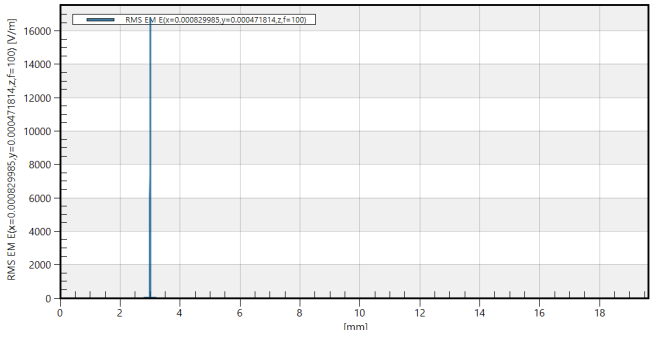

(b)

Figure 16: a) Overall field of the RMS of **E** analyzed along the neuron in the configuration with 10 MENPs orientated vrtically, as in Fig. 7b top. b) Overall field of the RMS of **E** analyzed along the neuron in the configuration with 10 MENPs orientated horizontally, as in Fig. 7b bottom.

Table 7 will show titration factors and time of the first spike of three different neuronal fibers. The choice is on fiber number 2 of fascicle 4, which is the one positioned between the ten MENPs, and on neuron 1 of fascicle 3 and neuron number 3 of fascicle 2. The last two fibers, formerly selected for the analysis of the configurations with five MENPs, have been preferred among all the neurons to give continuity in their characterization and analysis. As was noticed in the previous results, titration values needed to elicit the response of the fibers are higher in the horizontal configuration. Compared to the simulations with five MENPs, the needed stimulus amplitude is lower when stimulated with 10 MENPs in the vertical orientation, whereas, in the horizontal direction, the titration factor can either increase or decrease when incrementing the number of MENPs.

MENPs orientation	**Time of first spike [ms]**			**Titration factor**		
Vertical	8.5	8.06	8.06	101376	7936	2512
Horizontal	3.23	8.05	8.52	$1.42*10^6$	46592	286720

Table 7: Comparison of first spike's time and titration factor for three different fibers. Neuronal fibers are number 3 in fascicle 2, fiber number 1 in fascicle 3, and number 2 in fascicle 4, respectively. The orientation of the MENP varied in the two simulations.

The analysis will be concluded by showing the neuron response, an example is illustrated in Fig.17. For all the fibers in every simulation, the neuron behavior shows the characteristic shape of an action potential. Negligible distinctions were in the spiking, which instead reflects the different instants of the first spike. No influences of the MENPs configurations over the fiber response have been highlighted.

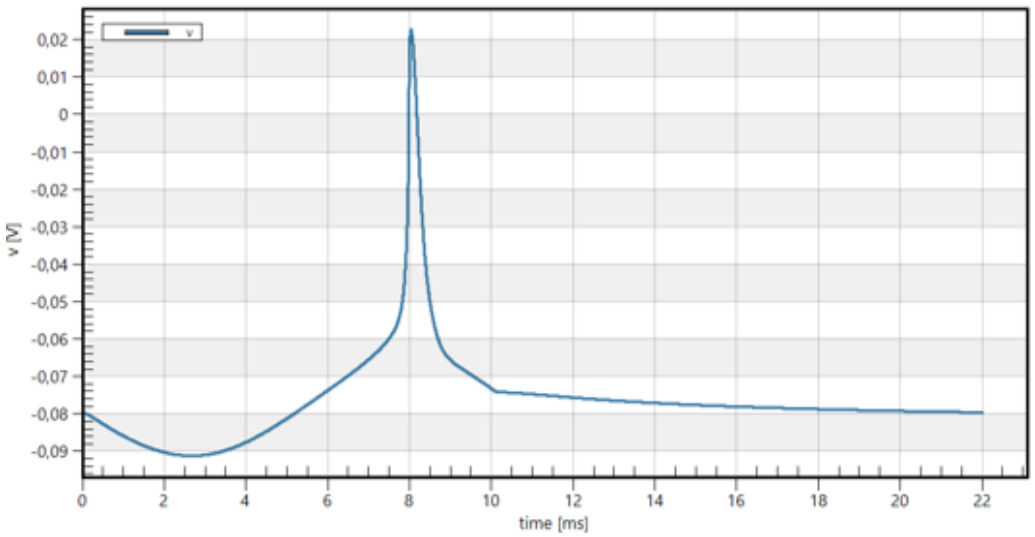

Figure 17: Typical neuron response.

4. Discussion

In the context of a growing interest towards innovative methods for peripheral nervous system (PNS) electric stimulation, magnetoelectric nanoparticles (MENPs) based approaches are gaining significance thanks to their peculiar potentials in terms of energy efficiency, minimal invasiveness, high-spatial resolution, and good biocompatibility [12], [14].

To effectively assess their behavior in the interaction with biological tissues and understand the main weakness to be strengthened, numerical methods can offer great support and, in perspective, can significantly boost the technological transfer into neurorehabilitation applications. This study fits into this field and wants to investigate by a numerical approach, the feasibility of recently developed MENPs in remotely modulating neural response and wirelessly tailoring nerve activity.

To do that, in this work, the local electric field distribution, the needed stimulus amplitude, and the neuron response for different MENPs configurations and MENP stimulating patterns in both simplified and realistic motor nerve models were numerically determined and compared.

The local electric field was visualized and analyzed in the simulations. The results showed that the EM field distribution is not influenced by the distance between the MENP and the axon or the shape of the delivered pulse, but it strongly depends on tissue inhomogeneity as well as MENPs arrangement (both number, position, and **E** field orientation), as demonstrated in Figs. 8, 13, 14, and 15a, 15b. Variation in MENPs configuration determines different interactions of the two polarities, affecting the EM field distribution. As expected, the highest values of **E** are obtained in the vicinity of the MENPs, fading out by increasing the distance from the source. It was highlighted that decreasing the distance or increasing the number of MENPs, increases the detected **E** field over the fiber. In addition, considering configurations with more than one MENP, a 90°-rotation of MENPs, which is achievable with a change in the orientation of the magnetic field source (i.e. coils), could be useful to further intensify the **E** field for the same voltage applied. Finally, the influence of tissue inhomogeneity over the **E** field was highlighted in the simulation with a single MENP placed on the border of a fascicle. The EM field was affected by the change of the medium, when passing from the extrafascicular to the intrafascicular tissue, generating an asymmetrical distribution.

Moreover, the overall field analyzed along the neuron has shown how punctual stimulation is feasible with MENP, allowing a very high spatial resolution. When decreasing the MENP–neuron distance or increasing the number of MENPs, the bell width of the RMS of E decreases as well. From the four case studies reported in Fig.9, it was shown how varying the MENP-axon distance from 3.5 to 0.5 um, determines a decrease in the 10% value of the maximum amplitude, with values starting from 14.8 to 1.8, respectively. The amplitude of the bell shape distribution was not calculated for the arrangements with more MENPs: an impulse-shaped distribution was visible from Figs. 16a, and 16b. The studies have demonstrated how spatial resolution is affected by both distance and the number of MENPs, confirming the potentiality of magnetoelectric nanoparticles in achieving better selectivity.

To analyze the temporal neuron response to varying electric stimuli used in neural stimulation, the Strength-Duration curve (SD), which is a graph relating the intensity of a threshold stimulus to its duration, was determined in different input signal conditions. The stimulus was either a sinusoid, as the typical pulse of a MENP, or a bipolar pulse, as commonly for the electrodes. The aim was to highlight the differences in the stimulus thresholds by changing the stimulating pattern. From the simulations, the threshold current was the titration factor value whereas the pulse duration was calculated as the reverse of the pulse frequency. Frequencies of 10, 25, 50, 75, 100, 250, 500, 750, and 1000 Hz have been considered. Both curves show the usual trend of the SD graphs: as the duration of a test stimulus increases, the intensity of the current required to activate a single fiber action potential decreases. Particularly, the threshold values for the sine pulse are higher than when stimulated with a bipolar pulse, for the same stimulus frequency. It follows the higher, even if not substantially different, effectiveness of the bipolar pulse over the sinusoidal pulse. However, the small dimensions of MENPs allow a decrease in the interposed distance between the stimulating source and the axon, placing the MENP as near as possible to the fibers, and counterbalancing the lack of intensity linked to the pulse shape. These results together encourage the need of future investigation to test the possibilities of stimulating with MENPs by triggering the neuron response with different pulse shapes.

The assessment of the neuron response reveals that the spiking activity of the neurons always reflected the characteristic shape of an action potential (AP), which is a fast, transitory, and propagating change of the resting membrane potential along the neural fiber. An AP has three phases, depolarization, overshoot, and

repolarization. It is preceded by a hypopolarization state and followed by a hyperpolarization. The membrane potential depends on the activity of the transmembrane ion channels. In the beginning, the neuron is at rest. The resting potential of the fiber is around -70 mV, stabilized by the K+ permeability. A short hypopolarization increases the Na+ conductivity, augmenting the membrane potential to the threshold value. The depolarization phase starts, opening the voltage-gated Na+ channels and causing a large influx of sodium ions. During depolarization, there is an increase of the potential inside the cell, until the electrochemical equilibrium for Na+ is reached. This phase of extremely positive potential is the overshoot phase. After the overshoot, the voltage-gated K+ channels open and the Na+ channels close, causing a large potassium efflux, decreasing the cell's electropositivity, and restoring the resting membrane potential. This phase is the repolarization phase. Before the membrane establishes again the values of membrane potential, there is hyperpolarization, a state in which the membrane potential is more negative than the default membrane potential. Before turning back into the resting state, the refractory period of the neuron's membrane, which is the time after an action potential is generated, limits the cell to fire again. Each described phase is visible in all the neuron responses analyzed. Particularly, results have confirmed that the AP is not influenced by the pulse shape or amplitude. The change in the fiber's spiking activity between the simplified and the realistic models can be due to different summation effects. The realistic model reflects better what happens in the neurons.

The titration factor gives information about the amplitude needed for the stimulus of the MENP. Its value is influenced by the MENP-fiber distance, the pulse polarization, the pulse shape, the number of MENPs, and the MENPs' orientation.

Both the MENP position and the MENP-neuron distance affect the titration factor. During the study, it was hypothesized a decrease in the titration factor by decreasing the MENP-axon distance. To investigate this influence, more simulations in a simplified environment have been run, considering distances up to 30 nm. However, the results of distances of 5, 10, 20, and 30 nm, have not been shown because not in line with the application of this study. As expected, all the results, even the not shown ones, confirmed the assumption: decreasing the MENP-axon distance, higher **E** field intensity is detected over the fiber, and as a consequence, lower stimulus amplitude is needed to reach the threshold. From 3.5 to 0.5 um of interposed distance, the titration value diminished noticeably, passing from 362 to 3.16. Similar results were expected when running simulations in a more realistic environment and stimulating with a single MENP. A decreasing trend of the titration factors was supposed when moving the MENP from the nerve's border towards the inside of the fascicle, considering also the extrafascicular position and the fascicle's border. Contrary to the supposed idea, the titration factor was higher with the MENP positioned on the fascicle's border than when placed in the extrafascicular space. As an example, titration values necessary to activate one of the fibers were $3.67*10^6$, 382976, 475136, and 313344 for the MENP placed near the border of the nerve, extrafascicularly, on the border of a fascicle, and intrafascicular, respectively. Generally, when the MENP was placed on the nerve's border, titration factors of the fibers of all the fascicles were of the order of 10^6 or 10^7. The lowest needed values for every neuron were instead observed with the MENP placed inside a fascicle. Then, depending on the relative position of the MENP and the single axon, the stimulus amplitude differed noticeably. However, all the neurons displayed a need for higher stimulus intensity when stimulated with the MENP placed in the extrafascicular space than when on the border of one fascicle. This outlying behavior can be due to the deformation of the **E** field distribution influenced by tissue inhomogeneity, as visible in Fig. 13.

During the study, it was evidenced the relevance of the number of MENPs and their orientation on the titration factors. As expected, the needed amplitude value to reach the threshold potential decreases by increasing the number of MENPs. The trend was visible in the simulations, where the MENPs number was incremented from 1 to 10 and lower titration factors were needed to elicit the axon potential. Considering a neuronal fiber, the titration factor decreased from 47872 to 2512 when stimulated with a single MENP or ten MENPs placed intrafascicular. A further decrease in the titration value was supposed when arranging the nanoparticles in a horizontal direction. In fact, as before-mentioned, a rotation of 90° in MENPs configurations, i.e. simulating the rotation of the orientation of the magnetic field eliciting the ME effect, determined an intensification in the **E** field amplitude peak. As a consequence, a lower needed stimulus amplitude to elicit the neuron response was expected for higher EM values. However, results highlight an opposite trend. The titration factor increased with MENPs orientated horizontally than when vertically oriented, both in configurations with five and ten MENPs. As an example, for the same fiber mentioned before, the needed stimulus amplitude increased from 2512 to 286720 from the vertical to the horizontal orientation. Moreover, the node of the first spike, not reported in this study, changed for almost every neuronal fiber, affected by the MENPs orientation. It derives the importance of the location of the EM peak over the axon length over the titration value. As already described, the spatial resolution achievable with MENPs is very high. However, if the source is not well positioned, it derives lower effectiveness in the stimulation. As a consequence, it is of extreme importance to know how and where to position the nanoparticles in order to achieve stimulation with very high spatial resolution and great validity.

When stimulated with MENPs, the best location for the sources is close to a node of a fiber.

In the end, the stimulus polarization had a modest influence on the titration factor, inducing a slightly lower needed pulse amplitude when stimulated with the inverse polarization, than using the direct one. This difference is linked to the electrical activity of the fiber. As it is known, a hyperpolarizing pre-pulse can facilitate the action potential initiation induced by the depolarization pulse and could also enhance selectivity [35].

5. Conclusions

In summary, the computational approaches have proven the feasibility of using MENPs as tools for the electric stimulation of peripheral nerves. At first, simplified simulations demonstrated the influence of MENP-axon distance, the pulse shape, and the pulse polarization over the EM field distribution and the axon response. Results have shown how the EM field distribution shape is not affected by any of the investigated components, but have highlighted the great impact of the MENP-axon distance over the amplitude of the peak of the **E** field distribution, and the overall field analyzed along the neuron. Simulations have shown how punctual stimulation is feasible with MENP, allowing a very high spatial resolution. Particularly, it was highlighted that, to achieve highly desirable spatial resolution and obtaining electric field intensity feasible to nerve stimulation, great attention should be paid to MENPs positioning in the vicinity of the nerve fiber, as all these desirable aspects are less under control when increasing the distance. The MENP capability to induce an action potential in the nerve, already observed in experimental and in vitro studies, was confirmed, and the response of the nerve was characterized. It was demonstrated how the MENP-axon distance, the pulse shape, and its polarization don't have any influence on the action potential shape, but the dependence of the variation of the time of the first spike on the stimulus frequency was evidenced. Finally, the information about the amplitude needed for the stimulus of the MENP was analyzed. As expected, results confirmed how the pulse amplitude necessary to reach the threshold increases by increasing the MENP–axon distance. Moreover, it was investigated how the pulse shape and the pulse polarization affect the needed pulse amplitude. Future work can address the feasibility of different stimulating patterns and pulse shapes with MENPs. Once the investigation has emphasized the nerve response and the EM distribution in a simplified environment, the study continued in a more realistic model, to better understand the impact of using MENPs as stimulating tools. Simulations with one, five, or ten MENPs were run, and the results of the EM field distribution, nerve response, and titration factor were compared. It was demonstrated how the **E** field is affected by the number of MENPs together with their position and orientation, as well as the homogeneity or inhomogeneity of the medium. The needed pulse amplitude was compared between different simulations. As expected, its value decreases by increasing the number of MENPs. Some unattended results were useful in underlying the importance of the position where to place the MENPs for stimulation and the orientation of the magnetic field used to elicit the ME effect (here approximated by modifying MENP dipoles orientation). In fact, the high spatial resolution is not sufficient if the stimulation is applied to the wrong point along the nerve. In the future, studies can focus on the development of MENPs chains or nanostructures with organized MENPs in order to get a highly effective stimulation to the positions of the nodes, without losing spatial resolution. In the end, the neuron response was characterized, and the usual action potential shape was evidenced.

In conclusion, this study demonstrated the feasibility of using MENPs as tools for the stimulation of peripheral nerves, highlighting all their potentialities. A lot is still to be understood about their functioning, and future work will be needed. The application of this innovative technology in medicine and bio-robotics will address the current limitations and drawbacks of the actual stimulating approaches, giving rise to cutting-edge bio-hybrid interfaces between living and artificial systems.

Acknowledgements

The author wishes to thank ZMT Zurich MedTech AG (www.zmt.swiss) for providing SIM4Life software.

This work was supported by the project "Fit4MedRob- Fit for Medical Robotics, Piano Nazionale Complementare (PNC) –PNC0000007".

References

[1] Krishnan Chakravarthy, Andrew Nava, Paul J. Christo, and Kayode Williams. Review of Recent Advances in Peripheral Nerve Stimulation (PNS). *Current Pain and Headache Reports*, 20(11):60, November 2016.

[2] C. Lee S. Lee Y. Cho, J. Park. Recent progress on peripheral neural interface technology towards bioelectronic medicine. *Bioelectron. Med., vol. 6, fasc. 1*, 2020.

[3] S. Chakrabarty C. Russell, A. D. Roche. Peripheral nerve bionic interface: a review of electrodes. *Int. J. Intell. Robot. Appl., vol. 3, fasc. 1*, page 11–18, 2019.

[4] Simone Romeni, Giacomo Valle, Alberto Mazzoni, and Silvestro Micera. Tutorial: a computational framework for the design and optimization of peripheral neural interfaces. *Nature Protocols*, 15(10):3129–3153, October 2020. Number: 10 Publisher: Nature Publishing Group.

[5] Pedrocchi A. Ambrosini E., Bejarano C. N. Sensors for motor neuroprosthetics: Current applications and future directions. *In Emerging Theory and Practice in Neuroprosthetics. edited by Ganesh R. Naik , and Yina Guo. Hershey, PA: IGI Global,*, pages 38–64, 2014.

[6] Aikaterini D. Koutsou, Susanna Summa, Bilal Nasser, Josefina Gutierrez Martinez, and Muthukumaran Thangaramanujam. Upper Limb Neuroprostheses: Recent Advances and Future Directions. In José L Pons and Diego Torricelli, editors, *Emerging Therapies in Neurorehabilitation*, volume 4, pages 207–233. Springer Berlin Heidelberg, Berlin, Heidelberg, 2014. Series Title: Biosystems & Biorobotics.

[7] del Ama A.J. et al. Koutsou A.D., Moreno J.C. Advances in selective activation of muscles for non-invasive motor neuroprostheses. *J NeuroEngineering Rehabil 13*, page 56, 2016.

[8] Lilach Bareket-Keren and Yael Hanein. Novel interfaces for light directed neuronal stimulation: advances and challenges. *International Journal of Nanomedicine*, 9(Suppl 1):65–83, May 2014.

[9] Catarina Dias, Domingos Castro, Miguel Aroso, João Ventura, and Paulo Aguiar. Memristor-Based Neuromodulation Device for Real-Time Monitoring and Adaptive Control of Neuronal Populations. *ACS Applied Electronic Materials*, 4(5):2380–2387, May 2022.

[10] Attarad Ali, Hira Zafar, Muhammad Zia, Ihsan ul Haq, Abdul Rehman Phull, Joham Sarfraz Ali, and Altaf Hussain. Synthesis, characterization, applications, and challenges of iron oxide nanoparticles. *Nanotechnology, Science and Applications*, 9:49–67, August 2016. Publisher: Dove Press.

[11] Brittany L. Banik, Pouria Fattahi, and Justin L. Brown. Polymeric nanoparticles: the future of nanomedicine. *Wiley Interdisciplinary Reviews. Nanomedicine and Nanobiotechnology*, 8(2):271–299, 2016.

[12] S. Kopyl, R. Surmenev, M. Surmeneva, Y. Fetisov, and A. Kholkin. Magnetoelectric effect: principles and applications in biology and medicine– a review. *Materials Today Bio*, 12:100149, September 2021.

[13] Armin Kargol, Leszek Malkinski, and Gabriel Caruntu. Biomedical Applications of Multiferroic Nanoparticles. In Leszek Malkinski, editor, *Advanced Magnetic Materials*. InTech, May 2012.

[14] Sakhrat Khizroev. Technobiology's Enabler: The Magnetoelectric Nanoparticle. *Cold Spring Harbor Perspectives in Medicine*, 9(8):a034207, August 2019.

[15] K. L. Kozielski, A. Jahanshahi, H. B. Gilbert, Y. Yu, Ö. Erin, D. Francisco, F. Alosaimi, Y. Temel, and M. Sitti. Nonresonant powering of injectable nanoelectrodes enables wireless deep brain stimulation in freely moving mice. *Science Advances*, 7(3):eabc4189, January 2021.

[16] Marta Pardo and Sakhrat Khizroev. Where do we stand now regarding treatment of psychiatric and neurodegenerative disorders? Considerations in using magnetoelectric nanoparticles as an innovative approach. *WIREs Nanomedicine and Nanobiotechnology*, 14(3), May 2022.

[17] Rakesh Guduru, Ping Liang, J. Hong, Alexandra Rodzinski, Ali Hadjikhani, Jeffrey Horstmyer, Ernest Levister, and Sakhrat Khizroev. Magnetoelectric 'spin' on stimulating the brain. *Nanomedicine (London, England)*, 10(13):2051–2061, 2015.

[18] Tyler Nguyen, Jianhua Gao, Ping Wang, Abhignyan Nagesetti, Peter Andrews, Sehban Masood, Zoe Vriesman, Ping Liang, Sakhrat Khizroev, and Xiaoming Jin. In Vivo Wireless Brain Stimulation via Non-invasive and Targeted Delivery of Magnetoelectric Nanoparticles. *Neurotherapeutics: The Journal of the American Society for Experimental NeuroTherapeutics*, 18(3):2091–2106, July 2021.

[19] Ali Hadjikhani, Alexa Rodzinski, Ping Wang, Abhignyan Nagesetti, Rakesh Guduru, Ping Liang, Carolyn Runowicz, Sina Shahbazmohamadi, and Sakhrat Khizroev. Biodistribution and clearance of magneto-electric nanoparticles for nanomedical applications using energy dispersive spectroscopy. *Nanomedicine*, 12(15):1801–1822, August 2017.

[20] Esra Neufeld, Antonino Mario Cassará, Hazael Montanaro, Niels Kuster, and Wolfgang Kainz. Functionalized anatomical models for EM-neuron Interaction modeling. *Physics in Medicine and Biology*, 61(12):4390–4401, June 2016.

[21] Andreas Christ, Wolfgang Kainz, Eckhart G Hahn, Katharina Honegger, Marcel Zefferer, Esra Neufeld, Wolfgang Rascher, Rolf Janka, Werner Bautz, Ji Chen, Berthold Kiefer, Peter Schmitt, Hans-Peter Hollenbach, Jianxiang Shen, Michael Oberle, Dominik Szczerba, Anthony Kam, Joshua W Guag, and Niels Kuster. The virtual family—development of surface-based anatomical models of two adults and two children for dosimetric simulations. *Physics in Medicine Biology*, 55(2):N23, dec 2009.

[22] FDA and IT'IS Foundation. Mida model v1.0. April 2015.

[23] IT'IS Foundation. Ella hand v3.0. January 2021.

[24] Serena Fiocchi, Emma Chiaramello, Alessandra Marrella, Giulia Suarato, Marta Bonato, Marta Parazzini, and Paolo Ravazzani. Modeling of core-shell magneto-electric nanoparticles for biomedical applications: Effect of composition, dimension, and magnetic field features on magnetoelectric response. *PLOS ONE*, 17(9):e0274676, September 2022.

[25] Soutik Betal, Binita Shrestha, Moumita Dutta, Luiz F. Cotica, Edward Khachatryan, Kelly Nash, Liang Tang, Amar S. Bhalla, and Ruyan Guo. Magneto-elasto-electroporation (MEEP): In-vitro visualization and numerical characteristics. *Scientific Reports*, 6(1):32019, August 2016.

[26] Amine M. Samoudi, Stefan Kampusch, Emmeric Tanghe, Jozsef C. Széles, Luc Martens, Eugenijus Kaniusas, and Wout Joseph. Numerical modeling of percutaneous auricular vagus nerve stimulation: a realistic 3D model to evaluate sensitivity of neural activation to electrode position. *Medical & Biological Engineering & Computing*, 55(10):1763–1772, October 2017.

[27] P. Wang et al. Colossal magnetoelectric effect in core-shell magnetoelectric nanoparticles. *Nano Lett*, 20(8):5765–5772, 2020.

[28] Baumgartner C Neufeld E Lloyd B Gosselin MC Payne D Klingenböck A Kuster N Hasgall PA, Di Gennaro F. It'is database for thermal and electromagnetic parameters of biological tissues. Version 4.1, February 2022.

[29] J. Patrick Reilly, Vanda T. Freeman, and Willard D. Larkin. Sensory Effects of Transient Electrical Stimulation - Evaluation with a Neuroelectric Model. *IEEE Transactions on Biomedical Engineering*, BME-32(12):1001–1011, December 1985.

[30] M. Stefano, F. Cordella, A. Loppini, S. Filippi, and L. Zollo. A Multiscale Approach to Axon and Nerve Stimulation Modeling: A Review. *IEEE Transactions on Neural Systems and Rehabilitation Engineering*, 29:397–407, 2021.

[31] JD Sweeney, JT Mortimer, and Dominique Durand. Modeling of mammalian myelinated nerve for functional neuromuscular stimulation in Proc 9th Ann Conf. volume 9, pages 1577–1578, January 1987.

[32] Cameron C. McIntyre, Andrew G. Richardson, and Warren M. Grill. Modeling the Excitability of Mammalian Nerve Fibers: Influence of Afterpotentials on the Recovery Cycle. *Journal of Neurophysiology*, 87(2):995–1006, February 2002.

[33] Jessica L. Gaines, Kathleen E. Finn, Julia P. Slopsema, Lane A. Heyboer, and Katharine H. Polasek. A model of motor and sensory axon activation in the median nerve using surface electrical stimulation. *Journal of Computational Neuroscience*, 45(1):29–43, August 2018.

[34] Carl H. Lubba, Yann Le Guen, Sarah Jarvis, Nick S. Jones, Simon C. Cork, Amir Eftekhar, and Simon R. Schultz. PyPNS: Multiscale Simulation of a Peripheral Nerve in Python. *Neuroinformatics*, 17(1):63–81, January 2019.

[35] Bemin Ghobreal, Farzan Nadim, and Mesut Sahin. Selective neural stimulation by leveraging electrophysiological differentiation and using pre-pulsing and non-rectangular waveforms. *Journal of Computational Neuroscience*, 50(3):313–330, August 2022. Publisher Copyright: © 2022, The Author(s), under exclusive licence to Springer Science+Business Media, LLC, part of Springer Nature.

Abstract in Lingua Italiana

Questo studio verifica la fattibilità dell'utilizzo delle particelle magnetoelettriche per la stimolazione dei nervi periferici del braccio. Lo scopo è quello di dimostrare la loro potenzialità come mezzi di stimolazione all'interno delle interfacce bioniche di prossima generazione degli arti umani superiori. L'analisi è stata effettuata attraverso tecniche computazionali, accoppiando simulazioni di tipo elettromagnetico e simulazioni che descrivono la dinamica neuronale. Sia modelli a geometria semplice che modelli a gometria complessa sono stati utilizzati nelle diverse simulazioni. In particolare, il livello di dettaglio, e quindi la complessità del modello stesso, è aumentata nelle varie simulazioni. All'inizio, una struttura semplice, costituita da una singola nanoparticella e un singolo assone, è stata oggetto di studio per analizzare l'influenza della nanoparticella stessa sulla risposta del neurone, approfondendo l'effetto di variazioni di distanza e modifiche sull'impulso di stimolazione. Successivamente è stata dimostrata l'adeguatezza dell'utilizzo delle nanoparticelle in un modello più realistico. I risultati suggeriscono la fattibilità dell'utilizzo di questa innovativa tecnica proposta, mettendo in risalto l'elevata risoluzione spaziale raggiungibile grazie a queste nanostrutture.

Parole chiave: Nanoparticelle Magnotelettriche, Stimolazione Elettrica dei Nervi, Tecniche Numeriche.